

Spectrally Matched Upconverting Luminescent Nanoparticles for Monitoring Enzymatic Reactions

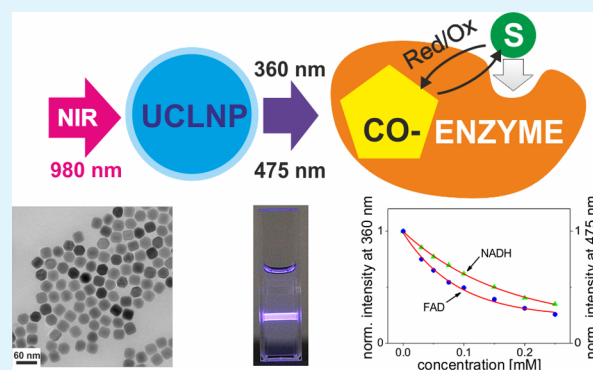
Stefan Wilhelm,[†] Melisa del Barrio,^{†,‡} Josef Heiland,[†] Sandy F. Himmelstoß,[†] Javier Galbán,[‡] Otto S. Wolfbeis,[†] and Thomas Hirsch^{*,†}

[†]Institute of Analytical Chemistry, Chemo- and Biosensors, University of Regensburg, 93040 Regensburg, Germany

[‡]Analytical Biosensors Group (GBA), Analytical Chemistry Department, Faculty of Science, Aragon Institute of Nanoscience (INA), University of Zaragoza, 50018 Zaragoza, Spain

ABSTRACT: We report on upconverting luminescent nanoparticles (UCLNPs) that are spectrally tuned such that their emission matches the absorption bands of the two most important species associated with enzymatic redox reactions. The core-shell UCLNPs consist of a β -NaYF₄ core doped with Yb³⁺/Tm³⁺ ions and a shell of pure β -NaYF₄. Upon 980 nm excitation, they display emission bands peaking at 360 and 475 nm, which is a perfect match to the absorption bands of the enzyme cosubstrate NADH and the coenzyme FAD, respectively. By exploiting these spectral overlaps, we have designed fluorescent detection schemes for NADH and FAD that are based on the modulation of the emission intensities of UCLNPs by FAD and NADH via an inner filter effect.

KEYWORDS: upconverting nanoparticles, enzymatic reactions, core-shell nanoparticles, upconversion, inner filter effect



INTRODUCTION

Upconverting luminescent nanoparticles (UCLNPs) are capable of converting near-infrared excitation light (NIR) into visible light.¹ The most efficient UCLNPs consist of lanthanide-doped sodium yttrium fluoride, which serves as a host material.² Ytterbium(III) ions, which act as sensitizers, absorb excitation light (usually with a wavelength of 980 nm) and then transfer energy to activator ions such as thulium(III).^{3,4} The relaxation of the excited states of activator ions to their ground states leads to the emission of photons shorter in wavelength than the excitation wavelength. This process is known as energy transfer upconversion.⁵ Sensitizer ions as well as activator ions usually are incorporated into an inorganic host lattice consisting of hexagonal-phase NaYF₄.⁶ This host is considered to be an ideal material for highly efficient UCLNPs due to its low phonon energy, which reduces multiphonon relaxation steps, and due to excited state lifetimes of up to a few milliseconds.⁷ Recently, highly photostable UCLNPs have been widely applied as contrast agents in biomedical imaging and biochemical sensing because autofluorescence of biological matter is largely reduced when using NIR light as an excitation source.^{8,9} Moreover, UCLNPs exhibit tunable emissions with narrow emission bandwidth and low cytotoxicity, and they can be incorporated into living cells,¹⁰ and used as nanolamps for the excitation of fluorophores.^{11,12} Their unique optical properties also have resulted in the design of near-infrared excitation light triggered drug release^{13,14} and quite new chemical sensing schemes.^{15,16}

Flavin adenine dinucleotide (FAD; a coenzyme) and nicotinamide adenine dinucleotide (NADH; a cosubstrate of

all dehydrogenases) are essential coreactants in numerous enzymatic redox reactions and in biological electron transport.¹⁷ For example, the NADH/NAD⁺ system transfers hydrogen atoms and electrons from one metabolite to another in many cellular redox reactions, and it is a known cofactor in more than 300 types of enzymatic reactions.¹⁸ Electrochemical methods have been reported to monitor NADH via oxidation to NAD⁺ during an enzymatic reaction.^{19,20} However, interferences by easily oxidizable other species are compromising their selectivity because direct electrochemical oxidation of NADH at a bare electrode requires a high overpotential.^{21,22} Electrode fouling due to the adsorption of stable reaction intermediates formed during the oxidation process is another issue.²³

To overcome these concerns, the electrode surface can be chemically modified, or mediators are being introduced. Lisdat et al. have reported on the concentration-dependent detection of NADH in the 20 μ M to 2 mM range by immobilizing CdSe/ZnS nanocrystals (quantum dots, QDs) on gold. Such a photoswitchable interlayer of QDs on a gold electrode allows for a spatially resolved read-out of the sensor surface at low electrode potentials (at \sim 0 V vs Ag/AgCl, 1 M KCl).²⁴ Most NADH-based enzymatic reactions are monitored via UV spectroscopy at 345 nm where NADH (in contrast to NAD⁺) displays fairly strong absorption. Numerous (clinical

Received: June 21, 2014

Accepted: August 4, 2014

Published: August 4, 2014

assays rely on this scheme that can be operated in the kinetic and in the end point mode.²⁵ Both FAD and NADH display intrinsic fluorescence. They can be excited by 450 nm light in the case of FAD (emission peaking at 512 nm) and by 350 nm light in the case of NADH (emission peaking at 450 nm).^{26,27} Unfortunately, NADH has a low quantum yield, and excitation in the UV causes biological samples such as serum to display strong autofluorescence.^{28,29} In addition, exciting light (350 nm) often is screened off due to an inner filter effect so that methods that work at much longer wavelengths are preferred. It was shown, for example, that NADH can be determined with the help of optical probes. Recently, Su et al. reported on albumin-coated CuInS₂ QDs emitting in the NIR for the determination of pyruvate using lactate dehydrogenase and NADH.³⁰ The fluorescence of the QDs with their emission peak at 680 nm is quenched by NADH. Willner et al. introduced CdSe/ZnS QDs modified with Nile Blue to monitor NADH-associated biocatalytic transformations.³¹ They were applied to metabolic studies on cancer cells, and anticancer agents were screened with respect to their effect on metabolism. Recently, Natrajan et al. reported on the application of upconverting two-wavelength phosphors (of unspecified size) to ratiometric monitoring of the enzyme pentaerythritol tetranitrate reductase via FRET (which we seriously doubt to occur given the distances involved in their system).³²

Here, we present detection schemes for the cosubstrate NADH and the coenzyme FAD, both of which are involved in numerous enzymatic reactions. Notably, it is making use of a single kind of UCLNPs. It relies on the modulation of either the blue or the UV emission of specifically designed UCLNPs by NADH and FAD, respectively. Most notably, NIR excitation (980 nm) can be applied, which is in striking contrast to practically all existing fluorometric methods.

EXPERIMENTAL SECTION

Chemicals. Yttrium(III) chloride hexahydrate (99.99%) and ytterbium(III) chloride hexahydrate (99.9%) were from Treibacher (www.treibacher.com). Thulium(III) chloride hexahydrate (99.99%), ammonium fluoride (ACS reagent $\geq 98.0\%$), sodium hydroxide (reagent grade $\geq 98.0\%$), poly(isobutylene-*alt*-maleic anhydride) (PMA; average $M_w \sim 6$ kDa), dodecylamine (98%), glucose oxidase from *Aspergillus niger* (type X-S, lyophilized powder, with an activity of 147.9 U·mg⁻¹ of lyophilized solid, EC 1.1.3.4), alcohol dehydrogenase from *Saccharomyces cerevisiae* (lyophilized powder, ≥ 300 U·mg⁻¹ protein), β -nicotinamide adenine dinucleotide hydrate ($\geq 99\%$), tris(hydroxymethyl)aminomethane (ACS reagent, $\geq 99.8\%$), semicarbazide hydrochloride ($\geq 99\%$), β -D(+)-glucose, 2-(*N*-morpholino)ethanesulfonic acid (MES), glycine (ACS reagent, $\geq 98.5\%$), boric acid (99.999%), flavin adenine dinucleotide (FAD) disodium salt ($\geq 95\%$), β -nicotinamide adenine dinucleotide (NADH), and reduced dipotassium salt were purchased from Sigma-Aldrich (www.sigmaaldrich.com). Oleic acid (technical grade 90%) and 1-octadecene (technical grade 90%) were from Alfa Aesar (www.alfa.com). All other reagents and organic solvents were of the highest grade available. Unless otherwise noted, all chemicals were used as received without further purification.

Instrumentation. Transmission electron microscopy (TEM) was performed using a 120 kV Philips CM12 microscope (www.fei.com). The particle size distributions of the nanocrystals were evaluated from the TEM images using the ImageJ software (<http://rsbweb.nih.gov/ij/>). The Zetasizer Nano-ZS from Malvern (www.malvern.com) was used for dynamic light scattering (DLS) experiments with intensity distribution weighted mode and for the measurement of the ζ -potential. X-ray powder diffraction (XRD) patterns with a resolution of 0.005° (2 θ) were collected using a Huber Guinier G670

diffractometer (www.xhuber.com) with a Cu source ($K\alpha$ radiation, $\lambda = 1.54060$ Å) operating at 40 kV and 30 mA. Flame-EOP inductively coupled plasma optical emission spectrometry (ICP-OES) was conducted with an instrument from Spectro (www.spectro.com) for the determination of the amount of rare-earth ions in the UCLNPs. All centrifugation steps were carried out using a Hettich Universal 320 centrifuge (www.hettichlab.com). A Sonorex Digitech DT255H ultrasonic bath from Bandelin (www.bandelin.com) was used. The upconversion luminescence spectra were recorded at room temperature with a luminescence spectrometer (LS 50 B) from PerkinElmer (www.perkinelmer.com) modified with a 980 nm continuous wave (CW) laser module (120 mW, ~ 15 W·cm⁻²) from Roithner (www.roithner-laser.com) for upconversion photoexcitation. Disposable cuvettes (1.5 mL, semimicro, Brand GmbH, Wertheim, Germany, www.brand.de) made from poly(methyl methacrylate) (PMMA) with an optical pathway of 1 cm were used for luminescence measurements. The upconversion luminescence lifetimes of the UCLNPs were measured using a home-built setup. The optical bandpass filter (FF02-470/100-25) for measuring a single emission band was bought from Semrock (www.semrock.com). The optical chopper system (MC2000 with two slot chopper blade MC1F2) was purchased from Thorlabs (www.thorlabs.com). The laser module (DH-980-200-3, 200 mW, ~ 130 W·cm⁻²) was bought from Picotronic (www.picotronic.com). To store and analyze the amplified signal a digital oscilloscope DSO 8204 from Voltcraft (www.voltcraft.ch) and LabVIEW-code (www.ni.com/labview) were used.

Synthesis of Nanoparticles Based on α -NaYF₄. Cubic-phase α -NaYF₄ nanocrystals were prepared by dissolving YCl₃·6H₂O (5 mmol) in ~ 5 mL of methanol using sonication. This solution was transferred into a 250 mL flask, mixed with 80 mL of oleic acid and 150 mL of 1-octadecene under an atmosphere of nitrogen and heated to 160 °C. A homogeneous, clear solution was formed after 30 min at 160 °C under vacuum. The reaction mixture was then cooled to room temperature and 50 mL of methanol containing NaOH (0.25 M) and NH₄F (0.4 M) was added at once. After the solution was stirred for 30 min at 120 °C, the resulting colloid suspension was heated to 240 °C for 30 min. After the solution cooled to room temperature, the UCLNPs were precipitated by addition of ~ 100 mL of ethanol and isolated via centrifugation at a relative centrifugal force (RCF; 1000g for 5 min). The pellet was washed several times by dispersing it in small amounts (~ 2 mL) of chloroform and cyclohexane, then precipitating them by the addition of a large excess (~ 20 mL) of ethanol and acetone. Finally, the purified UCLNPs were dispersed in 6 mL of oleic acid/1-octadecene (1/2 v/v) and used as the shell material for the preparation of core-shell UCLNPs.

Synthesis of Nanoparticles Based on β -NaYF₄ Doped with Yb³⁺/Tm³⁺ Ions. Hexagonal-phase, Yb³⁺/Tm³⁺-doped β -NaYF₄ nanoparticles were prepared by dissolving the salts of YCl₃·6H₂O (3.735 mmol), YbCl₃·6H₂O (1.25 mmol), and TmCl₃·6H₂O (0.015 mmol) in 5 mL of methanol by sonication.^{33,34} This solution was transferred into a 250 mL flask, mixed with 40 mL of oleic acid and 75 mL of 1-octadecene under an atmosphere of nitrogen, and heated to 160 °C. A homogeneous, clear solution was formed after 30 min at 160 °C under vacuum. The reaction mixture was then cooled to room temperature, and 50 mL of methanol containing NaOH (0.25 M) and NH₄F (0.4 M) was added at once. After the solution stirred for 30 min at 120 °C, the resulting colloid suspension was heated to reflux (~ 320 °C) for 20 min. The UCLNPs were precipitated by addition of ~ 100 mL of ethanol after cooling to room temperature. The procedure for cleaning was the same as described for the α -NaYF₄ nanocrystals. Finally, the purified UCLNPs were dispersed in 10 mL of cyclohexane and used as the core material for the preparation of core-shell UCLNPs.

Synthesis of Core-Shell Nanoparticles Based on β -NaYF₄(Yb³⁺/Tm³⁺)@NaYF₄. Hexagonal-phase core-shell UCLNPs based on β -NaYF₄(Yb³⁺/Tm³⁺)@NaYF₄ were prepared as follows.³⁵ 40 mL of oleic acid and 75 mL of 1-octadecene were mixed in a 250 mL flask and heated to 160 °C under an atmosphere of nitrogen. The mixture was cooled to 80 °C after 30 min at 160 °C under vacuum. β -NaYF₄(Yb³⁺/Tm³⁺) core UCLNPs dispersed in 10 mL of cyclohexane

were added, and the mixture was heated to 120 °C to evaporate the cyclohexane. After 30 min at 120 °C, the resulting colloid suspension was heated to reflux (~320 °C). α -NaYF₄ nanocrystals dispersed in 6 mL of oleic acid/1-octadecene (1/2 v/v) were quickly injected. Thereupon, the temperature dropped to ~300 °C. The mixture was stirred for another 15 min at reflux and cooled to room temperature. The core-shell UCLNPs based on β -NaYF₄(Yb³⁺/Tm³⁺)@NaYF₄ were precipitated by addition of ~100 mL of ethanol after cooling to room temperature. The procedure for cleaning was the same as described for the α -NaYF₄ nanocrystals. Finally, the purified UCLNPs were dispersed in 10 mL of cyclohexane.

Surface Modification Using an Amphiphilic Polymer Coating Strategy. The hydrophobic, oleate-coated, core-shell UCLNPs based on β -NaYF₄(Yb³⁺/Tm³⁺)@NaYF₄ were coated with an amphiphilic polymer poly(isobutylene-*alt*-maleic anhydride) (PMA) modified with dodecylamine to render them water dispersible. The synthesis of the amphiphilic polymer was reported previously.^{36,37} Hydrophobic core-shell UCLNPs (500 μ L; number of core-shell UCLNPs is $\sim 10^{14}$ as determined by ICP-OES) dispersed in chloroform were mixed together with 100 μ L of amphiphilic polymer solution (0.5 M) in a round-bottom flask. Afterward, 5 mL of chloroform was added, and sonication for 5 min was applied. Then, the chloroform was slowly evaporated under reduced pressure until the sample was completely dry. The remaining solid film in the flask was redispersed in ~5 mL of sodium borate buffer (SBB12; 50 mM; pH 12) under vigorous stirring until the solution turned clear. The resulting polymer-coated core-shell UCLNPs were preconcentrated using centrifuge filters (membrane: 100 kDa M_w cutoff, poly(ether sulfone) membrane, RCF: 870g for 15 min). Centrifugation was carried out until the sample solution had been concentrated to a volume of less than 250 μ L. The preconcentrated core-shell UCLNPs were further purified by centrifugation (RCF: 17000g for 30 min) and the resulting pellet redispersed in MES buffer (100 mM, pH 6.1).

Quantification of Ethanol. A Tris buffer solution (pH 8.7, 75 mM) containing 75 mM semicarbazide hydrochloride, 21 mM glycine, 24 mM NAD⁺, 300 U·mL⁻¹ alcohol dehydrogenase, and 1 μ M amphiphilic polymer-coated core-shell UCLNPs based on β -NaYF₄(Yb³⁺/Tm³⁺)@NaYF₄ was prepared. The upconversion emission intensity at 360 nm was measured (I_0). Thereafter, different amounts of ethanol in Tris buffer solution were added. The enzymatic oxidation of the ethanol took place immediately which resulted in a decrease of the emission intensity at 360 nm due to the production of NADH. The intensity (I) (after the enzymatic reaction stopped) was divided by I_0 and plotted against the mass concentration of ethanol.

Quantification of Glucose. A MES buffer solution (pH 6.1, 100 mM) containing 600 U·mL⁻¹ glucose oxidase (GOx) and 1 μ M polymer-coated core-shell UCLNPs based on β -NaYF₄(Yb³⁺/Tm³⁺)@NaYF₄ was prepared under nitrogen atmosphere. The solution (total volume of 700 μ L) was transferred into a cuvette and sealed with a layer of paraffin oil. The upconversion emission intensity at 475 nm was measured (I_0). Afterward, different amounts of glucose in MES buffer solution were added. The enzymatic oxidation of the glucose took place immediately, which resulted in an increase of the emission intensity at 475 nm due to the production of FADH₂. The intensity (I) (after the enzymatic reaction stopped) was divided by I_0 and plotted against the molar concentration of glucose.

RESULTS AND DISCUSSION

Preparation and Characterization of UCLNPs. UCLNPs consisting of a Yb³⁺/Tm³⁺-doped β -NaYF₄ core (with an inner diameter of 31.1 ± 1.0 nm) that was covered with a 3 nm shell of pure β -NaYF₄ were prepared.^{33,34} TEM images of α -NaYF₄, which were used as sacrificial nanoparticles for the synthesis of the shell, β -NaYF₄(Yb³⁺/Tm³⁺) core UCLNPs, and β -NaYF₄(Yb³⁺/Tm³⁺)@NaYF₄ core-shell UCLNPs are shown in Figure 1. Both the core-only and the core-shell UCLNPs exhibit a narrow size distribution (see Figure 2) and a purely

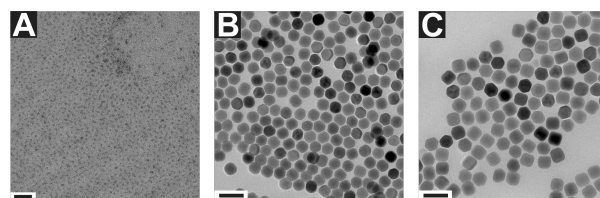


Figure 1. TEM images of (A) pure undoped α -NaYF₄ nanoparticles (scale bar: 20 nm), (B) β -NaYF₄(Yb³⁺/Tm³⁺) core-only UCLNPs (scale bar: 60 nm), and (C) β -NaYF₄(Yb³⁺/Tm³⁺)@NaYF₄ core-shell UCLNPs (scale bar: 60 nm).

hexagonal (β -phase) crystal structure (see Figure 3) according to the reference pattern (ICDD PDF #16-334).

The average diameter of core-shell UCLNPs based on β -NaYF₄(Yb³⁺/Tm³⁺)@NaYF₄ is 36.9 ± 1.4 nm as determined via evaluation of TEM images. In addition, the average nanocrystal size was calculated by evaluating the XRD data using Scherrer's equation to be ~3 nm for α -NaYF₄, ~30 nm for β -NaYF₄(Yb³⁺/Tm³⁺) core-only UCLNPs, and ~36 nm for β -NaYF₄(Yb³⁺/Tm³⁺)@NaYF₄ core-shell UCLNPs. These results are in good agreement with the TEM images. Scherrer's equation relates the size of submicrometer particles, or crystallites, in a solid to the broadening of a peak in a diffraction pattern.³⁸ The solvodynamic diameter of β -NaYF₄(Yb³⁺/Tm³⁺)@NaYF₄ core-shell UCLNPs dispersed in cyclohexane was determined by dynamic light scattering experiments to be ~35 nm with a polydispersity index (PDI) of 0.134, which is also in good agreement with the results of the TEM images and the XRD data. The concentration of UCLNPs in solution was determined by ICP-OES measurements. The calculation of the elemental composition agrees well with the data calculated from the amounts of lanthanide ions applied in synthesis (see Table 1).

A core-shell architecture was chosen because it increases the intensity of the upconversion luminescence (compared to the emission peak at 475 nm normalized to an Yb³⁺ concentration of ~8 mM) by a factor of ~60 (see Figure 4). An inert undoped shell of NaYF₄ minimizes the nonradiative deactivation of UCLNPs caused by solvent molecules, ligands, and surface defects because it spatially separates the lanthanide-doped core from the surrounding environment. Therefore, the upconversion luminescence lifetime of core-only and core-shell UCLNPs should be different.

The luminescence lifetime of core-only UCLNPs doped with Yb³⁺/Tm³⁺ (with their emission peaking at 470 nm in cyclohexane dispersion) increased from ~0.5 to ~0.9 ms in the case of the core-shell UCLNPs (see Figure 5). A monoexponential decay fitting based on the single exponential decay law was used. The increase in the average particle diameter, in luminescence intensity, and in luminescence lifetime along with the results of the ICP-OES measurements prove the presence of a core-shell architecture of the UCLNPs used here.³⁵ The decay curve of the core-only UCLNPs shows a deviation from a monoexponential decay because of experimental limitations. The recorded decay consists of two emissions (450 and 475 nm) which could not be separated by filters. Fitting it by a biexponential function results in lifetimes of 0.4 and 0.6 ms ($R^2 = 0.999$). The average value of 0.5 ms is in accordance to a monoexponential fit ($R^2 = 0.988$). For core-shell UCLNPs, there is no such deviation from monoexponential decay. Here the lifetime is estimated to 0.9 ms ($R^2 = 0.999$).

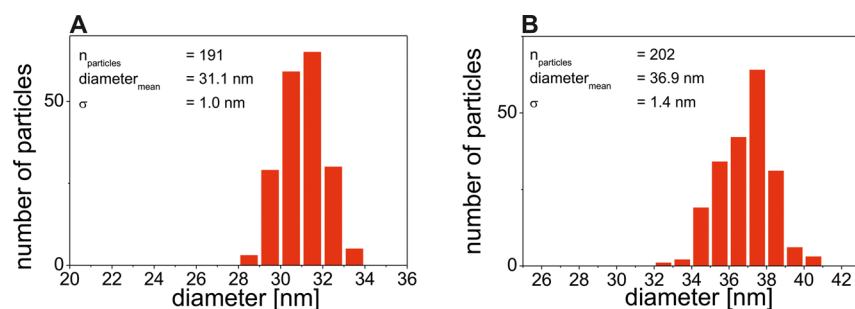


Figure 2. Size distribution histograms of (A) core-only UCLNPs (number of particles 191; mean diameter 31.1 nm; standard deviation 1.0 nm) based on β - $\text{NaYF}_4(\text{Yb}^{3+}/\text{Tm}^{3+})$ and (B) core-shell UCLNPs (number of particles 202; mean diameter 36.9 nm; standard deviation 1.4 nm) based on β - $\text{NaYF}_4(\text{Yb}^{3+}/\text{Tm}^{3+})@ \text{NaYF}_4$ as revealed from the corresponding TEM images.

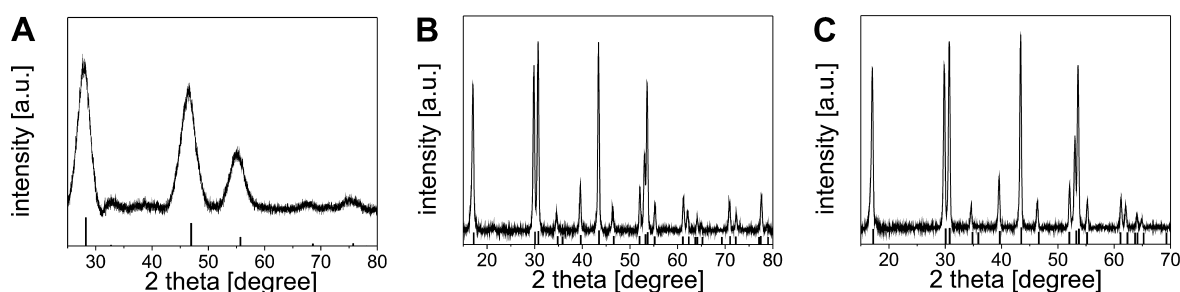


Figure 3. XRD patterns of: (A) pure undoped α - NaYF_4 nanoparticles (reference pattern ICDD PDF #77-2042, cubic phase), (B) β - $\text{NaYF}_4(\text{Yb}^{3+}/\text{Tm}^{3+})$ core-only UCLNPs, and (C) β - $\text{NaYF}_4(\text{Yb}^{3+}/\text{Tm}^{3+})@ \text{NaYF}_4$ core-shell UCLNPs (reference pattern ICDD PDF #16-334, hexagonal phase).

Table 1. Elemental Composition of α - NaYF_4 , β - $\text{NaYF}_4(\text{Yb}^{3+}/\text{Tm}^{3+})$ Core-Only UCLNPs, and β - $\text{NaYF}_4(\text{Yb}^{3+}/\text{Tm}^{3+})@ \text{NaYF}_4$ Core-Shell UCLNPs Determined by ICP-OES Measurements

| element | α - NaYF_4 [mol %] | core-only UCLNPs [mol %] | core-shell UCLNPs [mol %] |
|-----------|---------------------------------------|-----------------------------|------------------------------|
| yttrium | 100 | 75.4 \pm 0.1 | 85.2 \pm 0.1 |
| ytterbium | | 24.1 \pm 0.1 | 14.5 \pm 0.1 |
| thulium | | 0.5 \pm 0.1 | 0.3 \pm 0.1 |

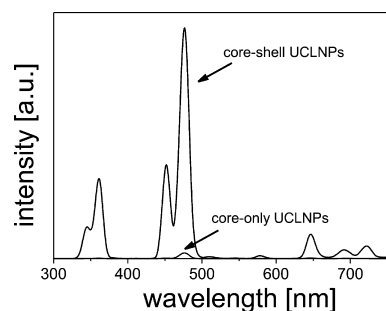


Figure 4. Upconversion luminescence spectra of β - $\text{NaYF}_4(\text{Yb}^{3+}/\text{Tm}^{3+})$ core-only and β - $\text{NaYF}_4(\text{Yb}^{3+}/\text{Tm}^{3+})@ \text{NaYF}_4$ core-shell UCLNPs dispersed in cyclohexane upon 980 nm CW laser excitation ($\sim 15 \text{ W}\cdot\text{cm}^{-2}$). Both spectra are normalized to an equal Yb^{3+} concentration (8.4 mM) as determined by ICP-OES analysis. An enhancement of the upconversion luminescence intensity (peak at 475 nm) by a factor of ~ 60 can be calculated.

In addition, the results demonstrate the beneficial effect of an undoped shell of pure NaYF_4 around the $\text{Yb}^{3+}/\text{Tm}^{3+}$ -doped core UCLNPs in terms of upconversion quantum yields (QYs).³⁹ These are, however, difficult to determine because several kinds of nonradiative deactivation (such as those caused by surface defects, ligands, and solvent) can occur. Although an

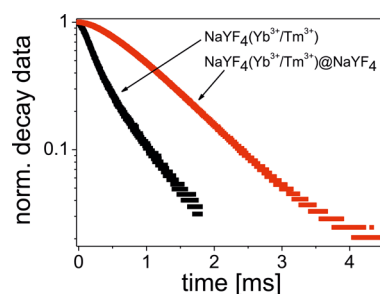


Figure 5. Upconversion luminescence lifetimes (emission at 470 nm) obtained for β - $\text{NaYF}_4(\text{Yb}^{3+}/\text{Tm}^{3+})$ core-only (~ 0.5 ms; black line) and β - $\text{NaYF}_4(\text{Yb}^{3+}/\text{Tm}^{3+})@ \text{NaYF}_4$ core-shell UCLNPs (~ 0.9 ms; red line) dispersed in cyclohexane upon 980 nm CW laser excitation (excitation power density $\sim 130 \text{ W}\cdot\text{cm}^{-2}$). The upconversion luminescence lifetime of core-shell UCLNPs dispersed in MES buffer (100 mM, pH 6.1) was the same as measured in cyclohexane viz. ~ 0.9 ms.

inert and undoped shell of NaYF_4 can minimize nonradiative deactivation processes, other effects are strongly affecting the accuracy in the determination of QYs. Moreover, their determination is not a trivial task, not the least because it is not defined for UCLNPs. If QYs are to be determined with an absolute method (for example, by using an integrating sphere), the Stokes-shifted emissions (at >1000 nm) also have to be taken into account, but these emissions are irrelevant in this context. Moreover, the QYs depend on the power density of the excitation (i.e., the laser source) because upconversion luminescence is a nonlinear phenomenon.

Surface Modification. Core-shell UCLNPs obtained in this way are hydrophobic and carry an oleate coating. In the next step, they were covered with the amphiphilic polymer poly(isobutylene-*alt*-maleic anhydride; PMA) that was previously modified with dodecylamine. This coating is remarkably

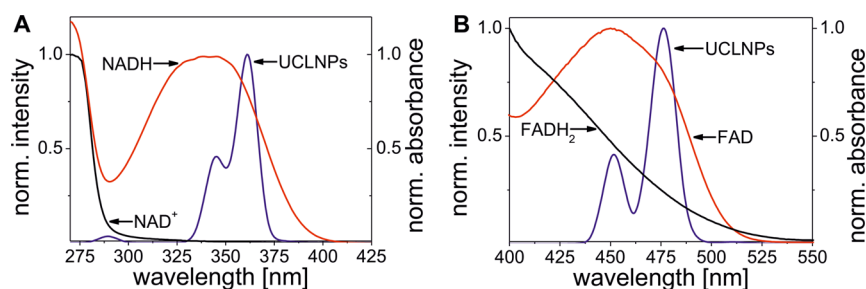


Figure 6. Normalized upconversion luminescence spectra of hydrophilic β - $\text{NaYF}_4(\text{Yb}^{3+}/\text{Tm}^{3+})@ \text{NaYF}_4$ core-shell UCLNPs dispersed in MES buffer (100 mM, pH 6.1) upon 980 nm CW laser excitation ($\sim 15 \text{ W}\cdot\text{cm}^{-2}$, blue line). (A) Normalized absorption spectra of NAD^+ (black line) and NADH (red line) in MES buffer. (B) Normalized absorption spectra of FADH_2 (black line) and FAD (red line) in MES buffer.

stable, probably due to the strong van der Waals interaction of the hydrophobic chains of the polymer with the hydrocarbon chains of oleate-coated UCLNPs. In addition, this coating renders initially hydrophobic UCLNPs water dispersible, obviously because its outward-directed polar side chains increase hydrophilicity.

Hydrophilic, polymer-coated UCLNPs can be colloidally dispersed in aqueous media after drying and purification. The hydrodynamic diameter of β - $\text{NaYF}_4(\text{Yb}^{3+}/\text{Tm}^{3+})@ \text{NaYF}_4$ core-shell UCLNPs (coated with PMA modified with dodecylamine) dispersed in 2-(*N*-morpholino)ethanesulfonate (MES; 100 mM) buffer of pH 6.1 is $\sim 61 \text{ nm}$ (PDI 0.124). Their ζ -potential is $\sim 47 \text{ mV}$ in MES buffer (100 mM, pH 6.1), and the colloid is stable for months, which is in agreement with earlier reports.^{36,37} This indicates that the surface-modified UCLNPs do not aggregate under these conditions.

Bioanalytical Application. Core-shell UCLNPs used in this work exhibit emission bands matching the absorption bands of both NADH and FAD. The normalized UV luminescence (peaking at 360 nm) of $\text{Yb}^{3+}/\text{Tm}^{3+}$ -doped core-shell UCLNPs upon 980 nm continuous wave (CW) laser excitation at a power density of $\sim 15 \text{ W}\cdot\text{cm}^{-2}$ is shown in Figure 6. It can be seen that it nicely matches the absorption band of NADH. The normalized visible (blue) luminescence of UCLNPs (peaking at 475 nm) overlaps the absorption band of FAD. These two upconversion luminescence bands are the result of electronic transitions from the $^1\text{D}_2$ to the $^3\text{H}_6$, and from the $^1\text{G}_4$ to the $^3\text{H}_6$ state, respectively, of Tm^{3+} activator ions of UCLNPs.

Figure 7 shows the decrease in the intensity of the upconversion emission at 360 nm with increasing concentration of NADH, and also at 475 nm with increasing concentrations of

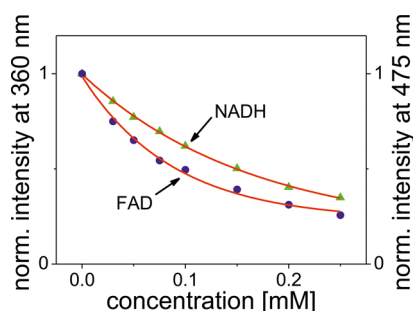


Figure 7. Decrease of upconversion luminescence intensities at 360 nm with increasing concentration of NADH and at 475 nm with increasing concentration of FAD due to the absorption of the redox cofactors upon 980 nm CW laser excitation ($\sim 15 \text{ W}\cdot\text{cm}^{-2}$).

FAD. This can be attributed to an inner filter effect, not the least because the decay time of the 470 nm emission ($\sim 0.9 \text{ ms}$) does not change on addition of FAD. An energy transfer between the UCLNPs and FAD and NADH can be excluded. Rather, the core-shell UCLNPs are acting as nanolamps whose emission is screened off. NADH can be detected in this way in the 30 to 150 μM concentration range, and FAD in the 30 to 100 μM range.

Next, two enzymatic reactions were studied to demonstrate the potential of this detection scheme. In the first experiment, the NAD^+ -associated oxidation of ethanol by alcohol dehydrogenase in Tris buffer solution of pH 8.7 was monitored in the presence of UCLNPs, which were found to remain completely inert. This reaction involves the oxidation of ethanol to form acetaldehyde (ethanal) along with NADH. Although NAD^+ does not absorb light at 360 nm, NADH is a strong absorber that can attenuate the emission at 360 nm, as can be seen in Figure 8A. Ethanol can be quantified by this method in the concentration range from 0.5 to 2.7 $\text{mg}\cdot\text{L}^{-1}$.

In an experiment involving the coenzyme FAD, we have monitored the enzymatic oxidation of β -D-glucose by glucose oxidase (GOx) to form D-glucono-1,5-lactone in MES buffer solution of pH 6.1 in the presence of UCLNPs. In this case, the situation is reversed in that the absorber (FAD) initially is present in high concentration but is converted to a less-absorbing species (FADH_2) in the course of the reaction. As a result, the emission peaking at 475 nm increases over time. Glucose can be determined by this method in the 20 to 200 μM glucose concentration range, as can be seen in Figure 8B.

CONCLUSIONS

In summary, it is demonstrated that core-shell UCLNPs based on β - $\text{NaYF}_4(\text{Yb}^{3+}/\text{Tm}^{3+})@ \text{NaYF}_4$ with their two emission peaks at 360 and 475 nm can be used to fluorescently monitor the formation of NADH and the consumption of FAD during enzymatic reactions using 980 nm photoexcitation. Given the average distances between the nanoparticles (where luminescence is created) and the coenzymes in solution (which is far beyond any Förster distance), we conclude from luminescence lifetime measurements that the effect is the result of an inner filter effect. Rather, the UCLNPs act as a kind of nanolamps. The effect is exemplarily shown to enable enzymatic assays for glucose and ethanol in that the intensity of the emission of the core-shell UCLNPs is affected by either the formation of NADH or the consumption of FAD. Although the method presented here may not have the low limits of detection of the best methods known for determination of either NADH and FAD and its phosphorylated analogs, the method has other attractive features. NIR light is used for photoexcitation, which

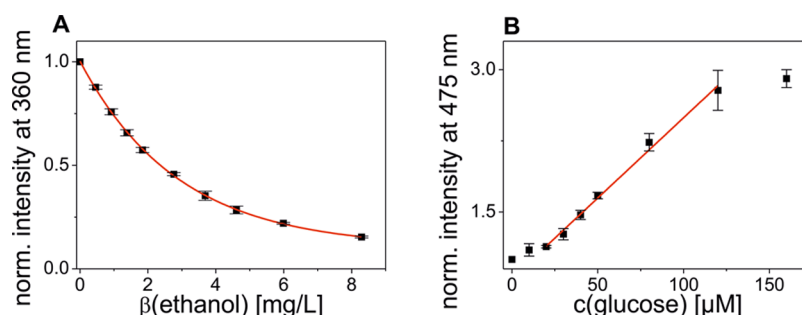


Figure 8. Quantification of (A) ethanol and (B) glucose using NADH- and FAD-related enzymatic reactions. Each data point reflects the average of three measurements, operated in the end point mode.

does not generate any autofluorescence of even complex biosamples at the wavelengths where NADH and FAD/FADH₂ display fluorescence. Photoexcitation in the NIR also is advantageous because this is the optical window of biomatter and blood. It is also noted that the same kind of nanoparticles may be used to monitor both NADH and FAD over time. Given the fact that this method is of general nature, we presume that it will be applicable to numerous other enzymatic processes that involve the NAD⁺/NADH (or NADP⁺/NADPH) or FAD/FADH₂ redox systems. One particularly attractive field of application may be in intracellular sensing where light scattering is strongly compromising the precision of conventional assays, and where photometry at 350 and 450 nm, respectively, is virtually impossible for the same reason.

AUTHOR INFORMATION

Corresponding Author

*Thomas Hirsch. E-mail: thomas.hirsch@ur.de.

Notes

The authors declare no competing financial interest.

ACKNOWLEDGMENTS

The authors thank Dr. C. Carillo-Carrion (Marburg) and Prof. W. J. Parak (Marburg) for developing the coating strategy with the amphiphilic polymer. M. del Barrio thanks the CSIC for funding for her JAE-Pre contract; J. Galbán thanks the MINECO (project CTQ2012-34774). This work was funded by the DFG (Bonn, Germany; project no. WO-669/12-1).

REFERENCES

- (1) Xu, C. T.; Zhan, Q.; Liu, H.; Somesfalean, G.; Qian, J.; He, S.; Andersson-Engels, S. Upconverting Nanoparticles for Pre-Clinical Diffuse Optical Imaging, Microscopy and Sensing: Current Trends and Future Challenges. *Laser Photonics Rev.* **2013**, *7*, 663–697.
- (2) Haase, M.; Schäfer, H. Upconverting Nanoparticles. *Angew. Chem., Int. Ed.* **2011**, *50*, 5808–5829.
- (3) Auzel, F. Upconversion and Anti-Stokes Processes with F and D Ions in Solids. *Chem. Rev.* **2004**, *104*, 139–174.
- (4) Pichaandi, J.; van Veggel, F. C. J. M.; Raudsepp, M. Effective Control of the Ratio of Red to Green Emission in Upconverting LaF₃ Nanoparticles Codoped with Yb³⁺ and Ho³⁺ Ions Embedded in a Silica Matrix. *ACS Appl. Mater. Interfaces* **2010**, *2*, 157–164.
- (5) Yang, Y. Upconversion Nanophosphors for Use in Bioimaging, Therapy, Drug Delivery and Bioassays. *Microchim. Acta* **2014**, *181*, 263–294.
- (6) Schaer, M.; Crittin, M.; Kasmi, L.; Pierzchala, K.; Calderone, C.; Digigow, R. G.; Fink, A.; Forró, L.; Sienkiewicz, A. Multi-Functional Magnetic Photoluminescent Photocatalytic Polystyrene-based Micro- and Nano-Fibers Obtained by Electrospinning. *Fibers* **2014**, *2*, 75–91.
- (7) Zhao, J.; Lu, Z.; Yin, Y.; McRae, C.; Piper, J. A.; Dawes, J. M.; Jin, D.; Goldys, E. M. Upconversion Luminescence with Tunable Lifetime in NaYF₄:Yb,Er Nanocrystals: Role of Nanocrystal Size. *Nanoscale* **2013**, *5*, 944–952.
- (8) Zhang, J.; Li, B.; Zhang, L.; Jiang, H. An Optical Sensor for Cu(II) Detection with Upconverting Luminescent Nanoparticles as an Excitation Source. *Chem. Commun.* **2012**, *48*, 4860–4862.
- (9) Mader, H. S.; Link, M.; Achatz, D. E.; Uhlmann, K.; Li, X.; Wolfbeis, O. S. Surface-Modified Upconverting Microparticles and Nanoparticles for Use in Click Chemistries. *Chem.—Eur. J.* **2010**, *16*, 5416–5424.
- (10) Cheng, L.; Wang, C.; Liu, Z. Upconversion Nanoparticles and Their Composite Nanostructures for Biomedical Imaging and Cancer Therapy. *Nanoscale* **2012**, *5*, 23–37.
- (11) Del Barrio, M.; de Marcos, S.; Cebolla, V.; Heiland, J.; Wilhelm, S.; Hirsch, T.; Galbán, J. Enzyme-Induced Modulation of the Emission of Upconverting Nanoparticles: Towards a New Sensing Scheme for Glucose. *Biosens. Bioelectron.* **2014**, *59*, 14–20.
- (12) Vetrone, F.; Naccache, R.; Zamarrón, A.; Juarranz de la Fuente, A.; Sanz-Rodríguez, F.; Martínez Maestro, L.; Martín Rodríguez, E.; Jaque, D.; García Solé, J.; Capobianco, J. A. Temperature Sensing Using Fluorescent Nanothermometers. *ACS Nano* **2010**, *4*, 3254–3258.
- (13) Niu, N.; He, F.; Ma, P.; Gai, S.; Yang, G.; Qu, F.; Wang, Y.; Xu, J.; Yang, P. Up-Conversion Nanoparticle Assembled Mesoporous Silica Composites: Synthesis, Plasmon-Enhanced Luminescence, and Near-Infrared Light Triggered Drug Release. *ACS Appl. Mater. Interfaces* **2014**, *6*, 3250–3262.
- (14) Wang, H.; Liu, Z.; Wang, S.; Dong, C.; Gong, X.; Zhao, P.; Chang, J. MC540 and Upconverting Nanocrystal Coloaded Polymeric Liposome for Near-Infrared Light-Triggered Photodynamic Therapy and Cell Fluorescent Imaging. *ACS Appl. Mater. Interfaces* **2014**, *6*, 3219–3225.
- (15) Achatz, D.; Ali, R.; Wolfbeis, O. Luminescent Chemical Sensing, Biosensing, and Screening Using Upconverting Nanoparticles. In *Luminescence Applied in Sensor Science*; Prodi, L.; Montalti, M.; Zaccaroni, N., Eds.; Topics in Current Chemistry; Springer: Berlin/Heidelberg, 2011; Vol. 300, pp 29–50.
- (16) Kannan, P.; Abdul Rahim, F.; Chen, R.; Teng, X.; Huang, L.; Sun, H.; Kim, D.-H. Au Nanorod Decoration on NaYF₄:Yb/Tm Nanoparticles for Enhanced Emission and Wavelength-Dependent Biomolecular Sensing. *ACS Appl. Mater. Interfaces* **2013**, *5*, 3508–3513.
- (17) Zhou, Y.; Xu, Z.; Yoon, J. Fluorescent and Colorimetric Chemosensors for Detection of Nucleotides, FAD and NADH: Highlighted Research during 2004–2010. *Chem. Soc. Rev.* **2011**, *40*, 2222.
- (18) Mayevsky, A.; Barbiro-Michaely, E. Use of NADH Fluorescence to Determine Mitochondrial Function in Vivo. *Int. J. Biochem. Cell Biol.* **2009**, *41*, 1977–1988.
- (19) Álvarez-González, M. I.; Saidman, S. B.; Lobo-Castañón, M. J.; Miranda-Ordieres, A. J.; Tuñón-Blanco, P. Electrocatalytic Detection of NADH and Glycerol by NAD⁺-Modified Carbon Electrodes. *Anal. Chem.* **2000**, *72*, 520–527.

(20) Malinauskas, A.; Ruzgas, T.; Gorton, L.; Kubota, L. T. A Reagentless Amperometric Carbon Paste based Sensor for NADH. *Electroanalysis* **2000**, *12*, 194–198.

(21) Tang, L.; Zeng, G.; Shen, G.; Zhang, Y.; Li, Y.; Fan, C.; Liu, C.; Niu, C. Highly Sensitive Sensor for Detection of NADH Based on Catalytic Growth of Au Nanoparticles on Glassy Carbon Electrode. *Anal. Bioanal. Chem.* **2009**, *393*, 1677–1684.

(22) Gros, P.; Comtat, M. A Bioelectrochemical Polypyrrole-Containing $\text{Fe}(\text{CN})_6^{3-}$ Interface for the Design of a NAD-Dependent Reagentless Biosensor. *Biosens. Bioelectron.* **2004**, *20*, 204–210.

(23) Jaegfeldt, H.; Kuwana, T.; Johansson, G. Electrochemical Stability of Catechols with a Pyrene Side Chain Strongly Adsorbed on Graphite Electrodes for Catalytic Oxidation of Dihydropyridinamide Adenine Dinucleotide. *J. Am. Chem. Soc.* **1983**, *105*, 1805–1814.

(24) Schubert, K.; Khalid, W.; Yue, Z.; Parak, W. J.; Lisdat, F. Quantum-Dot-Modified Electrode in Combination with NADH-Dependent Dehydrogenase Reactions for Substrate Analysis. *Langmuir* **2010**, *26*, 1395–1400.

(25) Passonneau, J. V.; Lowry, O. H. *Enzymatic Analysis: A Practical Guide*; Springer: Berlin/Heidelberg, 1993.

(26) Borisov, S. M.; Wolfbeis, O. S. Optical Biosensors. *Chem. Rev.* **2008**, *108*, 423–461.

(27) Georgakoudi, I.; Quinn, K. P. Optical Imaging Using Endogenous Contrast to Assess Metabolic State. *Annu. Rev. Biomed. Eng.* **2012**, *14*, 351–367.

(28) Wolfbeis, O. S.; Leiner, M. Mapping of the Total Fluorescence of Human Blood Serum as a New Method for Its Characterization. *Anal. Chim. Acta* **1985**, *167*, 203–215.

(29) Miller, J. N. Long-Wavelength and Near-Infrared Fluorescence: State of the Art, Future Applications, and Standards. In *Standardization and Quality Assurance in Fluorescence Measurements I*; Resch-Genger, U., Ed.; Springer Series on Fluorescence; Springer: Berlin/Heidelberg, 2008; Vol. 5, pp 147–162.

(30) Liu, S.; Shi, F.; Chen, L.; Su, X. Albumin Coated CuInS_2 Quantum Dots as a near-Infrared Fluorescent Probe for NADH, and Their Application to an Assay for Pyruvate. *Microchim. Acta* **2014**, *181*, 339–345.

(31) Freeman, R.; Gill, R.; Shweky, I.; Kotler, M.; Banin, U.; Willner, I. Biosensing and Probing of Intracellular Metabolic Pathways by NADH-Sensitive Quantum Dots. *Angew. Chem., Int. Ed.* **2009**, *48*, 309–313.

(32) Harvey, P.; Oakland, C.; Driscoll, M. D.; Hay, S.; Natrajan, L. S. Ratiometric Detection of Enzyme Turnover and Flavin Reduction Using Rare-Earth Upconverting Phosphors. *Dalton Trans.* **2014**, *43*, 5265.

(33) Wilhelm, S.; Hirsch, T.; Patterson, W. M.; Scheucher, E.; Mayr, T.; Wolfbeis, O. S. Multicolor Upconversion Nanoparticles for Protein Conjugation. *Theranostics* **2013**, *3*, 239–248.

(34) Qian, H.-S.; Zhang, Y. Synthesis of Hexagonal-Phase Core-Shell NaYF_4 Nanocrystals with Tunable Upconversion Fluorescence. *Langmuir* **2008**, *24*, 12123–12125.

(35) Johnson, N. J. J.; Korinek, A.; Dong, C.; van Veggel, F. C. J. M. Self-Focusing by Ostwald Ripening: A Strategy for Layer-by-Layer Epitaxial Growth on Upconverting Nanocrystals. *J. Am. Chem. Soc.* **2012**, *134*, 11068–11071.

(36) Pellegrino, T.; Manna, L.; Kudera, S.; Liedl, T.; Koktysh, D.; Rogach, A. L.; Keller, S.; Rädler, J.; Natile, G.; Parak, W. J. Hydrophobic Nanocrystals Coated with an Amphiphilic Polymer Shell: A General Route to Water Soluble Nanocrystals. *Nano Lett.* **2004**, *4*, 703–707.

(37) Sperling, R. A.; Pellegrino, T.; Li, J. K.; Chang, W. H.; Parak, W. J. Electrophoretic Separation of Nanoparticles with a Discrete Number of Functional Groups. *Adv. Funct. Mater.* **2006**, *16*, 943–948.

(38) Langford, J. I.; Wilson, A. J. C. Scherrer after Sixty Years: A Survey and Some New Results in the Determination of Crystallite Size. *J. Appl. Crystallogr.* **1978**, *11*, 102–113.

(39) Johnson, N. J. J.; van Veggel, F. C. J. M. Sodium Lanthanide Fluoride Core-Shell Nanocrystals: A General Perspective on Epitaxial Shell Growth. *Nano Res.* **2013**, *6*, 547–561.